Article

Proinflammatory Effects of Obesity in the Progression of Triple Negative Breast Cancer

Deok-Soo Son [1,*], Rosa Mistica C. Ignacio [1], Jubin Son [2], Eun-Sook Lee [3] and Samuel E. Adunyah [1]

[1] Department of Biochemistry, Cancer Biology, Neuroscience and Pharmacology, School of Medicine, Meharry Medical College, Nashville, TN 37208, USA
[2] Neuroscience Program, College of Arts and Sciences, The University of Tennessee, Knoxville, TN 37996, USA
[3] Department of Pharmaceutical Sciences, College of Pharmacy, Florida A&M University, Tallahassee, FL 32301, USA
* Correspondence: dson@mmc.edu
Received: 21 August 2024; Revised: 28 October 2024; Accepted: 2 December 2024; Published: 14 February 2025

Abstract: Obesity induces chronic inflammation and is associated with one-fifth of cancer deaths. Triple negative breast cancer (TNBC) has a higher death rate and increased proinflammatory chemokines compared to other breast cancer subtypes. Obesity leads to reduced overall survival in patients with TNBC. Here, we investigated if obesity-induced inflammation is involved in the progression of TNBC using cell line and animal models. Adipocyte-conditioned media (CM) increased cell viability, migration, and proinflammatory chemokines in mouse PY8119 TNBC cells, which reflect well human mesenchymal-like TNBC cells, compared to preadipocyte-CM. The *ob/ob* mice enhanced the progression of PY8119 cells by increasing the intensity of bioluminescence imaging, tumor volume and weight, and proinflammatory chemokines, compared to the wild-type mice. Furthermore, the immune contexture showed the higher levels of macrophage and CD4 cells in tumors of obese mice. Taken together, obesity may accelerate the progression of TNBC, revealing increased proinflammatory chemokines and altered immune contexture in the tumor microenvironment.

Keywords: triple negative breast cancer; obesity; adipocytes; chemokines

1. Introduction

Breast cancer (BC) is the most common type of women cancers, showing the second leading cause of cancer deaths. The five-year survival rate is 99.6% for localized BC, but only 31.9% for distant-stage BC [1]. Molecular subtypes of BC are widely classified as follows: estrogen receptor (ER) and/or progesterone receptor (PR) positive (+) and human epidermal growth factor receptor 2 (HER2) negative (–) luminal A (LA) subtype; ER and/or PR+ and HER2+ luminal B (LB) subtype; ER–, PR– and HER2+ HER2-enriched (HER2) subtype; ER–, PR– and HER2–basal-like (BL) subtype [2]. Particularly, triple-negative BC (TNBC) does not express ER, PR, and HER2, and shows aggressive tumorigenicity with risk of metastasis and recurrence followed by high mortality due to a lack of targets for treatment compared to non-TNBC subtypes [3–6]. Accordingly, finding specific therapeutic targets for TNBC is critical in treating TNBC. Chemokines have chemoattractant potential for cancer progression and metastasis. TNBC expressed dominantly proinflammatory chemokines, such as CXCL1 and 8, compared to non-TNBC [7].

The incidence of obesity has been increasing rapidly and globally [8]. Obesity contributes to one-fifth of cancer deaths [9]. Obesity is a risk factor for postmenopausal BC, and growing evidence indicates that abdominal obesity, known as central obesity, may increase risk for TNBC [10]. Meta-analysis on overall survival data between lean and obese TNBC patients showed that obesity is associated with poor overall survival of women with TNBC [11]. Cancer immunotherapy may be a promising treatment approach for TNBC under poor clinical outcome. Obesity has emerged to dampen anti-tumor immune response and increase immunotherapy-induced adverse events [12]. Therefore, obesity can harmfully affect the development of TNBC and cancer prognosis. Interestingly, overweight and obese cancer patients have better survival in diverse cancers, including esophageal, lung, colorectal, renal, and gastric cancers, and leukemia [13], presenting the obesity paradox in cancer. The relationship between obesity and cancer survival still faces ongoing issues, requiring further studies. Obesity induces chronic inflammation [14], appearing as a risk factor for many diseases, such as diabetes, cardiovascular disease, and cancer [15].

This study was designed to investigate if obesity-induced inflammation is involved in the progression of TNBC using cell line and animal models. In cell line model, we used the mouse fibroblast 3T3-L1 cell line to obtain preadipocyte- and adipocyte-conditioned media (CM) during adipogenesis. Furthermore, how adipocyte-CM affect the progression and chemokine signature of TNBC cells was evaluated when compared to preadipocyte-CM. In the animal model, ovariectomized mice were used to reflect a postmenopausal condition. We generated mouse TNBC PY8119Luc cells for bioluminescence imaging in an *ob/ob* mouse model and investigated if *ob/ob* mice had a greater effect on the tumor growth, proinflammatory chemokines, and immune contexture, compared to wild-type animals. These outcomes suggest that obesity contributes to the progression of TNBC by potentiating cell viability and migration, increasing proinflammatory chemokines, and altering immune contexture, showing the impact of obesity-induced inflammation.

2. Materials and Methods

2.1. Adipogenesis and Lipid Staining

The mouse fibroblast cell line 3T3-L1 (CL-173) was purchased from American Type Culture Collection (ATCC, Manassas, VA, USA). Cells were cultured in Dulbecco's Modified Eagle's medium (DMEM) with 10% calf serum (Invitrogen, Carlsbad, CA, USA) at 37 °C in a water-saturated atmosphere of 95% air and 5% CO_2, avoiding over-confluency (>70%) of the cells prior to differentiation. Differentiation was performed as described previously [16]. Undifferentiated and differentiated cells were washed with sterile phosphate-buffered saline (PBS) and cultured for an additional 48 h in complete DMEM media followed by centrifugation for preadipocyte- and adipocyte-conditioned media (CM) collection and storage at −80 °C for future use. All cell culture media were acquired from Invitrogen. The Oil Red O staining was used to confirm lipids in adipocytes. Briefly, we fixed cells in 4% paraformaldehyde in PBS for 15 min, washed the cells with PBS, stained cells with Oil Red solution for 1 h at room temperature, washed the cells with distilled water, and took photos of cells under microscopy (40×).

2.2. Cell Culture and Generation of Stable PY8119 Luciferase (PY8119Luc) TNBC Cell Line

To develop a C57BL/6J-based TNBC mouse model, we employed PY8119 cells obtained from spontaneously arising tumors in MMTV-PyMY (mouse mammary tumor virus promoter driven Polyoma middle T-antigen) transgenic C57BL/6 female mice [17]. PY8119 cells are derived from a mesenchymal-like (ML) murine mammary tumor cell line and are negative for expression of ER, PR, and HER2 [17,18]. C57BL/6-strain based PY8119 (ATCC® CRL-3278™) and BALB/c strain-based 4T1 (ATCC® CRL-2539™) cells were purchased from ATCC. Cell lines were grown in an incubator at 37 °C in a water-saturated atmosphere of 95% air and 5% CO_2. PY8119 cells were cultured in Ham's F-12K Medium supplemented with penicillin and streptomycin (each 100 U/mL) and 5% fetal bovine serum (FBS). Roswell Park Memorial Institute 1640 (RPMI 1640) Medium supplemented with penicillin and streptomycin (each 100 U/mL) and 10% FBS was used to culture 4T1 cells. PY8119Luc cells were generated for bioluminescence imaging by stable transfection of a luciferase vector (pGL4.51[luc2/CMV/Neo]; Promega Corporation, Madison, WI, USA) into parental PY8119 TNBC cells as described previously [19,20].

2.3. Cell Viability

Cell viability assay was performed using the cleavage of 3-(4,5-dimethylthiazol-2-yl)-2,5-diphenyltetrazolium bromide (MTT) to a colored product as described previously [19,20]. After 48 h incubation of cells with preadipocyte- and adipocyte-CM, respectively, cells were washed twice with phosphate-buffered saline (PBS) and then an MTT solution (1 mg/mL of phenol red-free media:PBS = 4:1) was added, followed by 3 h incubation of cells under protection from light. The MTT solution was removed, and isopropanol was added to fully dissolve the MTT color product followed by shaking the plates on an orbital shaker. After complete solubilization was confirmed with no precipitates of MTT products, optical density was measured at 595 nm wavelength using a microplate reader (Bio-Rad, Hercules, CA, USA). All experimental values were normalized to values obtained from vehicle controls without cells.

2.4. Cell Migration

Cell migration assay was performed as described previously [20]. Briefly, PY8119 cells (2×10^5 cells/mL in serum-free Ham's F-12K Medium supplemented with 1% BSA) were seeded in the 24-well Transwell cell culture insert (VWR Corp., Radnor, PA, USA). The bottom chamber contained 0.5 mL preadipocyte- and adipocyte-CM as a chemoattractant. After being incubated for 24 h, the cells that remained inside the insert were gently removed with a cotton swab. Migrating cells remaining on the filter were fixed with 3.7% formaldehyde and stained with 0.1% crystal violet. The cells were washed with PBS to remove overstaining. The number of migrating cells was counted under the microscope (400×) using five randomly chosen fields. Digital images were captured with BZ-X700 All-in-One Fluorescence Microscope (KEYENCE).

2.5. Western Blot

Whole-cell lysates were prepared, fractionated on SDS-polyacrylamide gels, and transferred to nitrocellulose membranes according to established procedures [7]. The following primary antibodies were used: Akt, Erk, and IκB and their phosphorylated forms (Cell Signaling Technology, Beverly, MA, USA). The protein bands were visualized by chemiluminescence detection kits (MilliporeSigma, St. Louis, MO, USA). Tubulin (TU-02, Santa Cruz Biotechnology, Dallas, TX, USA) was used as a loading control.

2.6. Data Analysis for Gene Expression Omnibus (GEO)

GEO data analysis was carried out by using publicly available microarray datasets deposited in the National Center for Biotechnology Information GEO database (http://www.ncbi.nlm.nih.gov/geo/ accessed on 25 Jan. 2019) as described in previous studies [21,22].

2.7. Polymerase Chain Reaction (PCR) Array

PCR array was performed as described in a previous study [20]. PCR array for customized mouse chemokines (CAMP10242) was designed and purchased from Qiagen (Frederick, MD, USA). Total RNA was isolated with the elimination of genomic DNA from TNBC cell samples. The reverse transcriptase reaction was performed at 42 °C for 15 min followed by 94 °C for 5 min. A real-time PCR reaction for chemokines and chemokine receptors was performed according to the manufacturer's instructions using a Bio-Rad CFX96 Touch Real-Time PCR System (Hercules, CA, USA) and the following two-step cycling program: 1 cycle at 95 °C for 10 min; and 40 cycles at 95 °C for 15 s and at 60 °C for 1 min. Based on raw data obtained, data analysis was performed according to instructions of the GeneGlobe Data Analysis Center (https://geneglobe.qiagen.com/us/analyze/) supplied by Qiagen website.

2.8. The ob/ob Mouse Model and Orthotopic Mammary Fat Pad Injection of PY8119Luc TNBC Cells

A mouse model and procedure were evaluated under guidelines approved by the Institutional Animal Care and Use Committee at Meharry Medical College and the NIH guide for the Care and Use of Laboratory Animals (#16-03-511). We employed the *ob/ob* mouse model bearing PY8119Luc TNBC cells for bioluminescence imaging. Ovariectomized wild-type (WT, C57BL/6J) and *ob/ob* mice (B6.V-Lepob/J) at 8 weeks age ± 3 days were obtained from Jackson Laboratory. Both mice were fed with normal diet and kept in a specific pathogen free animal housing facility which was maintained at 22 °C ± 2 °C and 40%–60% humidity under a 12:12 h light and dark cycle. The body weight gain was confirmed by approximately 2-fold difference between WT and *ob/ob* mice and PY8119Luc cells (3×10^6 cells/mouse) prepared in PBS:Matrigel with 50:50 ratio were administered into the 4th right mammary fat pad. Bioluminescence imaging was monitored on a weekly basis for detecting tumor growth. Briefly, mice were anesthetized with 3% isoflurane and were administered with D-luciferin (Cayman Chemical, Ann Arbor, MI, USA) intraperitoneally at 125 mg/kg, 5 min prior to acquisition of the image. Mice then were placed in the chamber of an In-Vivo MS FX PRO optical imaging system (Carestream, NY, USA) under anesthetized condition, and photons were collected for a period of 1 min. The luminescent intensity for the region of interest was quantified using Molecular Imaging software (Carestream). In addition, tumor volumes were calculated on a weekly basis after TNBC cell injection using the following formula: $(\text{length} \times \text{width}^2)/2$.

2.9. Enzyme-Linked Immunosorbent Assay (ELISA) for Chemokines

Keratinocyte chemoattractant (KC) levels in cell lysates and tumor tissues were measured using a murine KC ELISA kit (900-K127, PeproTech, Rocky Hill, NJ, USA) according to the manufacturer's instructions. The optical density of each well was determined at 405 nm wavelength with correction of 570 nm in a microplate reader.

2.10. Fluorescence-Activated Cell Sorting (FACS)

For single cell isolation, tumoral tissues were dissected to the size of approximate 1 mm^3 in the DMEM/F12 medium containing penicillin/streptomycin (each 100 U/mL), 10% FBS, collagenase (300 units/mL), and hyaluronidase (100 units/mL). Dissected tissues were digested at 37 °C for 30 min. After pipetting to dissociate cells and centrifugation at 300–400× *g* for 5 min, cell mixture was treated in the DMEM/F12 medium with dispase II (5mg/mL) and DNase I (0.1mg/mL) at 37 °C for 5 min. After centrifugation, the cell mixture was resuspended in 0.25% trypsin/EDTA for digestion at 37 °C for 5 min and was added with 5 mL DMEM/F12 medium with 10% FBS to neutralize trypsin. After centrifugation, cells were resuspended in the red blood cell lysis buffer (eBioscience™ 1X RBC Lysis Buffer, Thermo Fisher Scientific, Waltham, MA, USA) for 5 min at room temperature. After centrifugation, cells were washed twice with wash buffer (PBS containing 0.1% bovine serum albumin and 5 mM EDTA). Resuspended cells with staining buffer (PBS containing 1% bovine serum albumin and 1% EDTA) were filtered through the 40 μm cell strainer. Immune cell profiles in tumors were analyzed using a FACScan flow cytometer (BD Biosciences, San Jose, CA, USA) with the following specific antibodies for leukocyte subtypes: Alexa Fluor® 647 Rat Anti-Mouse F4/80 for detecting Mφ; PE Rat Anti-Mouse CD4 for detecting CD4 T cells; APC Rat Anti-Mouse CD8a for detecting CD8 T cells. FloJo software (Tree Star Inc., Ashland, OR, USA) was used to quantify the percentage of immune cells.

2.11. Statistical Analysis

Data were expressed as mean ± standard error of the mean (SEM) and analyzed by the Student's *t*-test to detect statistical significance ($p < 0.05$).

3. Results

3.1. Adipocyte-CM Potentiates the Progression of PY8119 TNBC Cells

We collected preadipocyte- and adipocyte-CM from adipogenesis of 3T3-L1 cells [16] and evaluated how these CM affect functional roles of PY8119 cells, a murine TNBC cell line [17,18]. After differentiation of 3T3-L1 cells into adipocytes, we confirmed lipids in adipocytes with Oil Red O staining (Figure 1A).

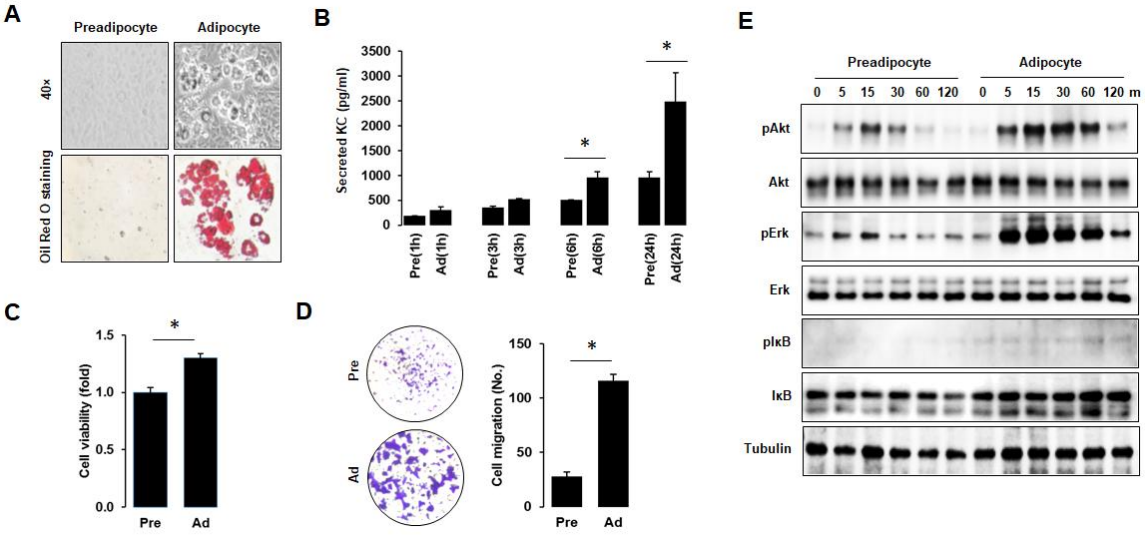

Figure 1. Effects of adipocyte-CM in PY8119 TNBC cells. (**A**) Adipogenesis of 3T3-L1 cells. Oil Red O staining confirmed lipids in adipocytes. (**B**) Time-course of secreted KC chemokines in PY8119 TNBC cells after application of preadipocyte- and adipocyte-CM by ELISA. (**C**) Cell viability of PY8119 TNBC cells after preadipocyte- and adipocyte-CM treatment. (**D**) Migration of PY8119 TNBC cells after preadipocyte- and adipocyte-CM treatment. (**E**) Comparison of Akt, Erk, and NF-κB activation in preadipocyte- and adipocyte-CM-

treated PY8119 TNBC cells by immunoblotting. Tubulin was used as a loading control. Pre: preadipocyte-CM; Ad: adipocyte-CM. Experiments were performed at least in triplicate and all data values were expressed as the mean ± SEM. * $p < 0.05$ as calculated by Student's *t*-test.

Human TNBC cell lines express high levels of proinflammatory chemokines, such as CXCL1 and CXCL8, compared with other subtypes [7]. As mice lack IL8/CXCL8, CXCL1–3 or CXCL5 are considered murine homologues for human CXCL8 [23]. Accordingly, we compared effects of preadipocyte- and adipocyte-CM on secretion of KC chemokines (CXCL1-3) in PY8119 cells. Adipocyte-CM induced more highly secreted KC chemokines in PY8119 TNBC cells compared to preadipocyte-CM (Figure 1B). Adipocyte-CM also increased cell viability and migration in PY8119 TNBC cells compared to preadipocyte-CM (Figure 1C,D). Furthermore, we compared Akt, Erk, and NF-κB activation between preadipocyte- and adipocyte-CM treated PY8119 TNBC cells. Both preadipocyte- and adipocyte-CM activated Akt and Erk in PY8119 TNBC cells without a critical activation of NF-κB (Figure 1E). The activation of Akt and Erk in PY8119 cells was greater in application of adipocyte-CM compared to that of preadipocyte-CM (Figure 1E).

3.2. Adipocyte-CM Induces Proinflammatory Chemokines in Murine TNBC Cells

TNBC exerts aggressive tumorigenicity and high mortality compared with other BC subtypes [3–6]. The chemokine network is involved in metastasis of breast cancer [24–26], emerging as the leading cause of mortality in cancer patients. As a result, we investigated whether chemokine signatures of PY8119 cells corroborate with those of human TNBC cells. We analyzed chemokine signatures in TNBC subtypes as follows: nine BL-TNBC, six ML-TNBC, and seven luminal androgen receptor (LAR)-TNBC cell lines from the GEO dataset (GSE12777) (Figure 2A). BL- and ML-TNBC cells expressed elevated levels of CXCL1 and CXCL8 compared with LAR-TNBC cells. Comparison of chemokine signatures between BL- and ML-TNBC cells revealed that BL-TNBC cells expressed higher levels of CXCL16, while ML-TNBC cells expressed higher levels of CCL20 and CXCL12 (Figure 2A). We also analyzed chemokine signatures in murine TNBC cells, PY8119 and 4T1 cells, using customized PCR array containing complementary sequences for mouse chemokine genes (Figure 2B). PY8119 cells expressed higher levels of CXCL12, while 4T1 cells expressed higher levels of CXCL16, CXCR3, and CXCR7 (Figure 2B). PY8119 cells showed similar chemokine signatures to those in human ML-TNBC cells, while 4T1 cells had similar signatures to those in human BL-TNBC cells. A recent study indicates that 4Tl cells show similarity with the BL- and immune-suppressed TNBC subtype [27]. We compared chemokine signatures between adipocyte-CM-treated PY8119 and 4T1 TNBC cells using PCR array (Figure 2C). Adipocyte-CM increased CXCL2, CXCL3, and CXCL5 in PY8119 cells and CXCL1 and CXCL2 in 4T1 cells (Figure 2C).

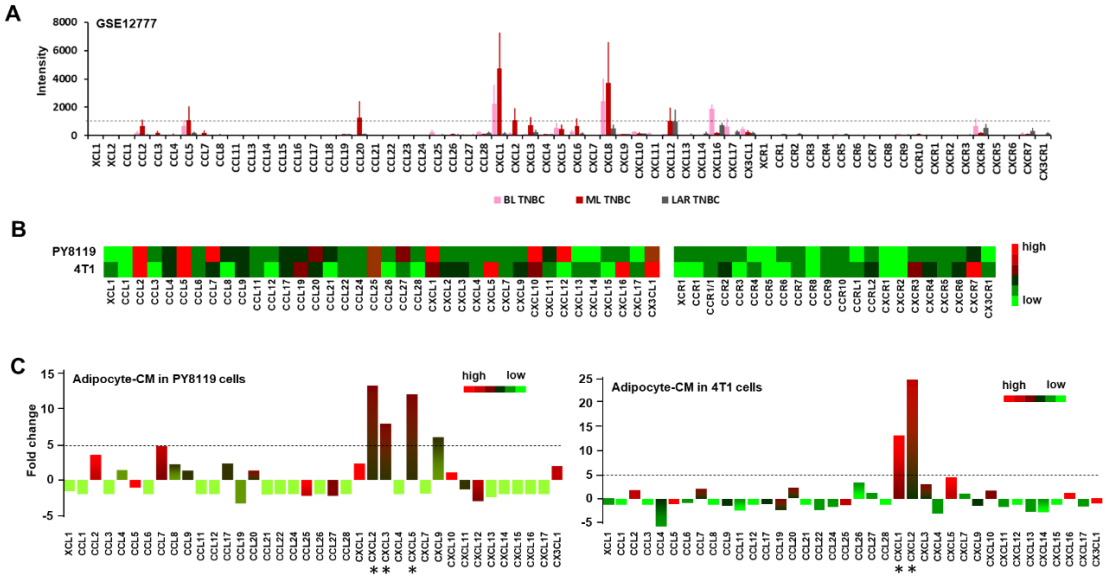

Figure 2. Chemokine signatures of TNBC cells and adipocyte-CM-induced chemokines in PY8119 TNBC cells. (**A**) Chemokine signatures in 9 basal-like (BL)-TNBC, 6 mesenchymal-like (ML)-TNBC, and 7 luminal androgen receptor (LAR)-TNBC cell lines from GEO dataset (GSE12777) analysis. Data values were expressed as the mean ± SEM. (**B**) Heatmap for chemokine and its receptors levels in mouse PY8119 and 4T1 TNBC cell lines using PCR array for mouse chemokine genes. Expression levels of chemokines and chemokine receptors were defined as

absent (light green), low (green) and high (red) based on average threshold cycles. (**C**) Comparison of chemokine signatures between PY8119 and 4T1 TNBC cells after 6 h adipocyte-CM treatment using PCR array. Highly expressed chemokines with a >5-fold increase (*) were recognized as a major chemokine responsive to adipocyte-CM.

3.3. The Ovariectomized ob/ob Female Mice Potentiate the Progression of PY8119 TNBC Cells

The *ob/ob* mouse has been served as an obese mouse model since its first discovery in 1949 [28]. We used ovariectomized *ob/ob* female mice fed normal diet to reflect a postmenopausal obese mouse model and explored tumorigenic parameters on the progression of PY8119 TNBC cells in an orthotopic mammary fat pad model (Figure 3). We confirmed body weights between WT and *ob/ob* female mice (Figure 3A). The *ob/ob* mice had approximately 2-fold greater weights compared to WT mice (Figure 3A). We generated PY8119Luc cells from parental PY8119 TNBC cells to monitor the tumor burden imaging. Bioluminescence imaging revealed that *ob/ob* mice had higher bioluminescence intensity compared to WT mice (Figure 3B,C). Accordingly, *ob/ob* mice had bigger tumor volumes and weights than WT mice (Figure 3D,E). The spleen weights of *ob/ob* mice were lower compared to those of WT mice (Figure 3F). There was a negative relationship between tumor and spleen weights in WT and *ob/ob* mice (Figure 3G). In addition, tumoral KC levels were higher in *ob/ob* mice compared to WT mice (Figure 3I).

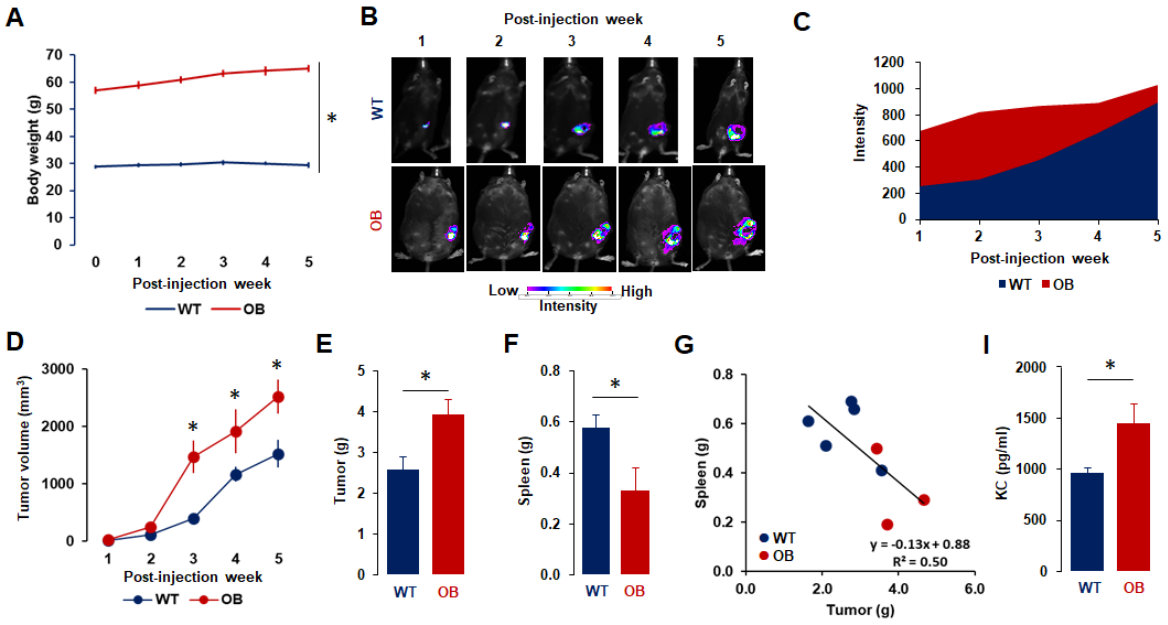

Figure 3. The progression of PY8119 TNBC cells in postmenopausal obese mouse model using an orthotopic mammary fat pad model. (**A**) Comparison of body weights between wild-type (WT, n = 5) and *ob/ob* (OB, n = 4) female mice. (**B**) Bioluminescence imaging for the tumor burden of PY8119 cell-bearing mice. Representative pictures were obtained from 5 WT and 4 OB mice. (**C**) Average intensity of bioluminescence imaging between WT and OB mice in an orthotopic mammary fat pad model. (**D**) Tumor volumes in WT and OB mice. (**E**) Tumor weights in 5 WT and 4 OB mice. (**F**) Spleen weights in 5 WT and 3 OB mice. (**G**) Negative relationship between tumor and spleen weights in 5 WT and 3 OB mice. (**I**) Tumoral KC levels in WT and OB mice assessed by ELISA. All mice were ovariectomized prior to performing the experiment to reflect postmenopausal status. Data values were expressed as the mean ± SEM. * $p < 0.05$ as calculated by Student's *t*-test compared with WT.

3.4. Obesity Induces Accumulation of Mφ and CD4 Cells in Immune Cell Contexture of Tumor Tissues

Because tumor infiltrating immune cells affect clinical outcomes, we evaluated immune cell infiltration in tumor tissues. FACS analysis revealed that the percentage of F4/80 as a Mφ marker was higher in tumors of *ob/ob* mice compared to those of wild-type mice (Figure 4A). Although the percentage of CD8 cells had no change in tumors of wild-type and *ob/ob* mice (Figure 4B), that of CD4 cells appeared to be higher in tumors of *ob/ob* mice compared to those of wild-type mice (Figure 4C).

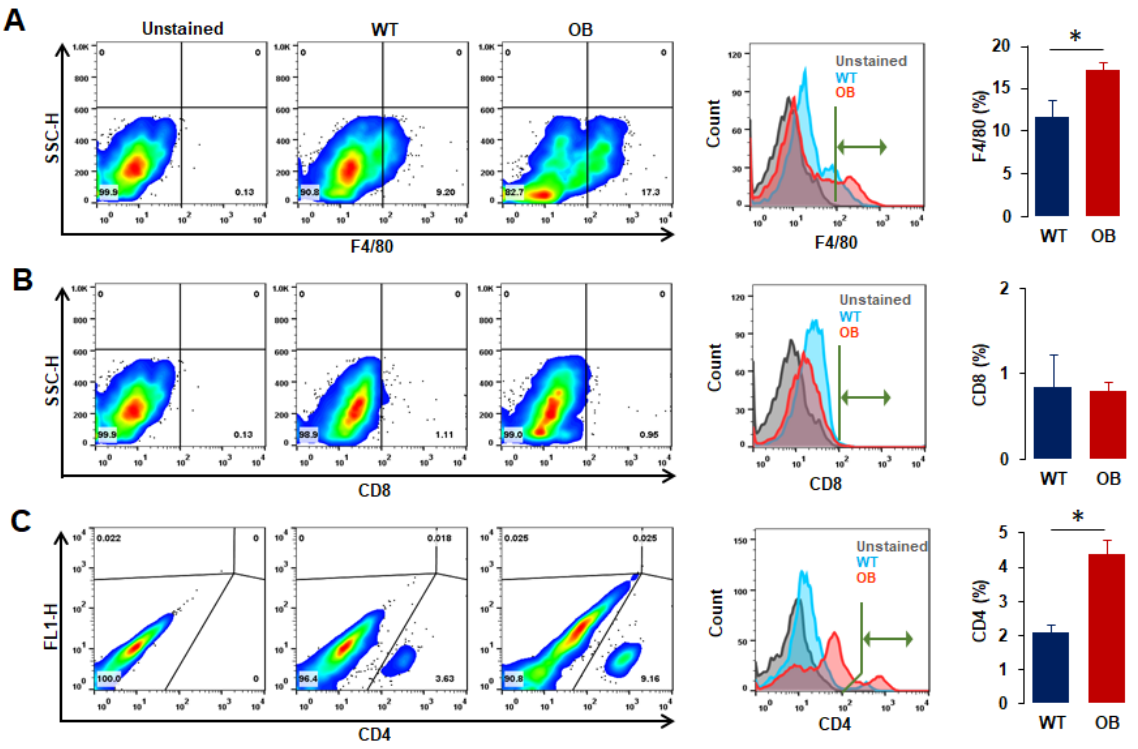

Figure 4. Analysis of flow cytometer on immune cells in tumor tissues from WT and OB mice with orthotopic mammary fat pad models. The comparative percentage of F4/80 (**A**), CD8 cells (**B**), and CD4 cells (**C**) in tumor tissues from wild-type (WT, n = 4) and *ob/ob* (OB, n = 3) female mice. Data values were quantified utilizing FloJo software. * $p < 0.05$ as calculated by Student's *t*-test compared to WT mice.

4. Discussion

The main findings in this study show that obesity may contribute to the progression of TNBC. This includes cancer cell growth and migration, increased proinflammatory chemokines like KC chemokines, and altered immune contexture in the tumor microenvironment, specifically showing increased tumoral infiltration of Mφ and CD4 cells.

Adipocyte-CM induced KC chemokines in PY8119 TNBC cells (Figure 1B) indicate that obesity may induce proinflammatory chemokines in TNBC cells, potentially resulting in increased tumorigenicity of TNBC. The results that adipocyte-CM increased cell viability and migration in PY8119 TNBC cells (Figure 1C,D) corroborate previous findings. Co-culture with adipocytes and adipocyte-CM increased cell proliferation and migration in human MDA-MB-231 ML-TNBC cells [29–36], human BT549 ML-TNBC cells [32], human SUM159PT ML-TNBC cells [37], human MDA-MB-468 BL-TNBC cells [38], human HCC38 BL-TNBC cells [35], human MDA-MB-453 LAR-TNBC cells [33], and murine 4T1 TNBC cells [39]. Based on these results, our findings also suggest that PY8119 TNBC cells are well suited for the adipocyte-induced cell viability and migration as observed in human TNBC cells. The facts that adipocyte-CM activated Akt and Erk in PY8119 TNBC cells (Figure 1C,D) are supported by previous studies. Adipocyte-CM activated Akt in human MDA-MB-231 ML-TNBC cells [30]. Akt signaling predictably is associated with obesity in premenopausal women, and Erk signaling significantly is predicted to associate obesity with TNBC in postmenopausal women [40]. Despite these limited data, our findings demonstrate that PY8119 TNBC cells share signaling pathways with those observed in human TNBC cells.

Adipocyte-CM-induced chemokines in murine TNBC cells are CXCR2 ligands, such as CXCL1–3 and CXCL5–8 (Figure 2C), which function as proangiogenic and tumorigenic chemokines [41,42]. Co-culture with adipocytes and adipocyte-CM increased CXCL8 levels in human MDA-MB-231 ML-TNBC cells [33,43] and human MDA-MB-453 LAR-TNBC cells [33]. As CXCL1–3 or CXCL5 are murine homologues for human CXCL8 [23], adipocyte-CM-induced CXCL2, CXCL3, and CXCL5 in PY8119 cells are consistent with the results from human TNBC cells. In addition to CXCL8, adipocyte-CM increased CCL20, CXCL2, and CXCL3 levels in human MDA-MB-231 ML-TNBC cells [44]. Based on chemokine signatures induced by adipocyte-CM, PY8119 and 4T1 TNBC cells reflect well the chemokine network for human TNBC cells.

The spleen weights of *ob/ob* mice were lower compared with those of WT mice (Figure 3F) as supported by other study [45]. At this point, it is unclear whether decreased spleen weight affected the progression of TNBC.

Tumoral KC levels were higher in *ob/ob* mice compared with WT mice (Figure 3I), paralleling with adipocyte-CM-induced chemokine signatures (Figures 1B and 2C). Tumor weights of PY230 BL-TNBC cells and 4T1 TNBC cells were increased in *ob/ob* mice [46] and high-fat induced obese mice [47], respectively, supporting our results of PY8119 ML-TNBC cells in *ob/ob* mice (Figure 3E). PY8119Luc cells generated in this study can be used to monitor the progression of TNBC in a time-dependent manner, reflecting the characteristics of human ML-TNBC in normal and obese states.

Immune cell contexture of tumor tissues from *ob/ob* mice indicates that obesity induces tumoral accumulation of Mφ and CD4 cells (Figure 4). Consistently, our previous studies showed that Mφ was highly accumulated in ovarian omental tumors of obese mice [48] and in breast tumor tissues of high-fat diet-induced obese mice [11]. In addition, CD4+ and CD25+ cells were increased in cancer-sentinel lymph nodes of obese mice bearing 4T1 TNBC cells [47]. Obesity induces mammary white adipose tissue expansion with an accumulation of Mφ, followed by a worse prognosis for breast cancer [14]. These results indicate that obesity-induced inflammation may promote tumoral infiltration of Mφ in the breast tumor microenvironment, probably affecting the prognosis of TNBC.

In conclusion, obesity may accelerate the progression of TNBC, promoting cancer cell viability and migration followed by tumor growth, increasing proinflammatory chemokines, and changing immune contexture in the breast tumor microenvironment, which display a critical role of obesity-induced inflammation in TNBC.

Author Contributions: Conceptualization, D.-S.S.; methodology, D.-S.S., R.M.C.I., J.S. and E.-S.L.; software, D.-S.S., R.M.C.I. and J.S.; validation, D.-S.S., E.-S.L. and S.E.A.; formal analysis, D.-S.S., R.M.C.I., J.S. and E.-S.L.; investigation, D.-S.S., R.M.C.I. and J.S.; resources, D.-S.S., E.-S.L. and S.E.A.; data curation, D.-S.S., R.M.C.I., J.S. and E.-S.L.; writing—original draft preparation, D.-S.S.; writing—review and editing, D.-S.S., R.M.C.I., J.S., E.-S.L. and S.E.A; visualization, D.-S.S.; supervision, D.-S.S.; project administration, D.-S.S.; funding acquisition, D.-S.S., E.-S.L. and S.E.A. All authors have read and agreed to the published version of the manuscript.

Funding: This research was funded, either in whole or in part, by the National Institutes of Health (NIH) through the following grants: R01ES031282 (E.-S.L.), SC1CA200519 (D.-S.S.), U54MD007586 (S.E.A.), U54CA163069 (D.-S.S., S.E.A.), and ACS DICRIDG-21-071-01-DICRIDG (D.-S.S., S.E.A.).

Institutional Review Board Statement: The study was conducted according to the NIH guide for the Care and Use of Laboratory Animals, and approved by the Institutional Animal Care and Use Committee at Meharry Medical College (eProtocol #16-03-511 and date of approval: 19 Feb. 2016).

Informed Consent Statement: Not applicable.

Data Availability Statement: Publicly available microarray datasets (GSE12777) is deposited in the National Center for Biotechnology Information GEO database (http://www.ncbi.nlm.nih.gov/geo/ accessed on 25 Jan. 2019).

Conflicts of Interest: The authors declare no conflicts of interest with the contents of this article.

References

1. Cancer Stat Facts: Female Breast Cancer. Available online: https://seer.cancer.gov/statfacts/html/breast.html (accessed on 15 Feb. 2024).
2. Wiechmann, L.; Sampson, M.; Stempel, M.; Jacks, L.M.; Patil, S.M.; King, T.; Morrow, M. Presenting features of breast cancer differ by molecular subtype. *Ann. Surg. Oncol.* **2009**, *16*, 2705–2710. https://doi.org/10.1245/s10434-009-0606-2.
3. Wu, X.; Baig, A.; Kasymjanova, G.; Kafi, K.; Holcroft, C.; Mekouar, H.; Carbonneau, A.; Bahoric, B.; Sultanem, K.; Muanza, T. Pattern of Local Recurrence and Distant Metastasis in Breast Cancer by Molecular Subtype. *Cureus* **2016**, *8*, e924. https://doi.org/10.7759/cureus.924.
4. Shim, H.J.; Kim, S.H.; Kang, B.J.; Choi, B.G.; Kim, H.S.; Cha, E.S.; Song, B.J. Breast cancer recurrence according to molecular subtype. *Asian Pac. J. Cancer Prev.* **2014**, *15*, 5539–5544.
5. Moo, T.A.; McMillan, R.; Lee, M.; Stempel, M.; Ho, A.; Patil, S.; El-Tamer, M. Impact of molecular subtype on locoregional recurrence in mastectomy patients with T1-T2 breast cancer and 1-3 positive lymph nodes. *Ann. Surg. Oncol.* **2014**, *21*, 1569–1574. https://doi.org/10.1245/s10434-014-3488-x.
6. Herrera, A.C.; Panis, C.; Victorino, V.J.; Campos, F.C.; Colado-Simão, A.N.; Cecchini, A.L.; Cecchini, R. Molecular subtype is determinant on inflammatory status and immunological profile from invasive breast cancer patients. *Cancer Immunol. Immunother.* **2012**, *61*, 2193–2201. https://doi.org/10.1007/s00262-012-1283-8.
7. Ignacio, R.M.C.; Gibbs, C.R.; Lee, E.S.; Son, D.S. The TGFα-EGFR-Akt signaling axis plays a role in enhancing proinflammatory chemokines in triple-negative breast cancer cells. *Oncotarget* **2018**, *9*, 29286–29303. https://doi.org/10.18632/oncotarget.25389.
8. Blüher, M. Obesity: global epidemiology and pathogenesis. *Nat. Rev. Endocrinol.* **2019**, *15*, 288–298. https://doi.org/10.1038/s41574-019-0176-8.
9. Williams, S.C. Link between obesity and cancer. *Proc. Natl. Acad. Sci. USA* **2013**, *110*, 8753–8754. https://doi.org/10.1073/pnas.1308182110.
10. Agurs-Collins, T.; Ross, S.A.; Dunn, B.K. The Many Faces of Obesity and Its Influence on Breast Cancer Risk. *Front. Oncol.* **2019**, *9*, 765. https://doi.org/10.3389/fonc.2019.00765.
11. Son, D.S.; Done, K.A.; Son, J.; Izban, M.G.; Virgous, C.; Lee, E.S.; Adunyah, S.E. Intermittent Fasting Attenuates Obesity-Induced Triple-Negative Breast Cancer Progression by Disrupting Cell Cycle, Epithelial-Mesenchymal

Transition, Immune Contexture, and Proinflammatory Signature. *Nutrients* **2024**, *16*, 2101. https://doi.org/10.3390/nu16132101.
12. Naik, A.; Monjazeb, A.M.; Decock, J. The Obesity Paradox in Cancer, Tumor Immunology, and Immunotherapy: Potential Therapeutic Implications in Triple Negative Breast Cancer. *Front. Immunol.* **2019**, *10*, 1940. https://doi.org/10.3389/fimmu.2019.01940.
13. Lee, D.H.; Giovannucci, E.L. The Obesity Paradox in Cancer: Epidemiologic Insights and Perspectives. *Curr. Nutr. Rep.* **2019**, *8*, 175–181. https://doi.org/10.1007/s13668-019-00280-6.
14. Kolb, R.; Zhang, W. Obesity and Breast Cancer: A Case of Inflamed Adipose Tissue. *Cancers* **2020**, *12*, 1686. https://doi.org/10.3390/cancers12061686.
15. Włodarczyk, M.; Nowicka, G. Obesity, DNA Damage, and Development of Obesity-Related Diseases. *Int. J. Mol. Sci.* **2019**, *20*, 1146. https://doi.org/10.3390/ijms20051146.
16. Kabir, S.M.; Lee, E.S.; Son, D.S. Chemokine network during adipogenesis in 3T3-L1 cells: Differential response between growth and proinflammatory factor in preadipocytes vs. adipocytes. *Adipocyte* **2014**, *3*, 97–106. https://doi.org/10.4161/adip.28110.
17. Gibby, K.; You, W.K.; Kadoya, K.; Helgadottir, H.; Young, L.J.; Ellies, L.G.; Chang, Y.; Cardiff, R.D.; Stallcup, W.B. Early vascular deficits are correlated with delayed mammary tumorigenesis in the MMTV-PyMT transgenic mouse following genetic ablation of the NG2 proteoglycan. *Breast Cancer Res.* **2012**, *14*, R67. https://doi.org/10.1186/bcr3174.
18. Biswas, T.; Gu, X.; Yang, J.; Ellies, L.G.; Sun, L.Z. Attenuation of TGF-β signaling supports tumor progression of a mesenchymal-like mammary tumor cell line in a syngeneic murine model. *Cancer Lett.* **2014**, *346*, 129–138. https://doi.org/10.1016/j.canlet.2013.12.018.
19. Ignacio, R.M.C.; Lee, E.S.; Son, D.S. Potential Roles of Innate Immune Chemokine and Cytokine Network on Lipopolysaccharide-Based Therapeutic Approach in Ovarian Cancer. *Immune Netw.* **2019**, *19*, e22. https://doi.org/10.4110/in.2019.19.e22.
20. Ignacio, R.M.C.; Lee, E.S.; Wilson, A.J.; Beeghly-Fadiel, A.; Whalen, M.M.; Son, D.S. Obesity-Induced Peritoneal Dissemination of Ovarian Cancer and Dominant Recruitment of Macrophages in Ascites. *Immune Netw.* **2018**, *18*, e47. https://doi.org/10.4110/in.2018.18.e47.
21. Ignacio, R.M.C.; Lee, E.S.; Wilson, A.J.; Beeghly-Fadiel, A.; Whalen, M.M.; Son, D.S. Chemokine Network and Overall Survival in TP53 Wild-Type and Mutant Ovarian Cancer. *Immune Netw.* **2018**, *18*, e29. https://doi.org/10.4110/in.2018.18.e29.
22. Ignacio, R.M.C.; Gibbs, C.R.; Kim, S.; Lee, E.S.; Adunyah, S.E.; Son, D.S. Serum amyloid A predisposes inflammatory tumor microenvironment in triple negative breast cancer. *Oncotarget* **2019**, *10*, 511–526. https://doi.org/10.18632/oncotarget.26566.
23. Hol, J.; Wilhelmsen, L.; Haraldsen, G. The murine IL-8 homologues KC, MIP-2, and LIX are found in endothelial cytoplasmic granules but not in Weibel-Palade bodies. *J. Leukoc. Biol.* **2010**, *87*, 501–508. https://doi.org/10.1189/jlb.0809532.
24. Zielińska, K.A.; Katanaev, V.L. The Signaling Duo CXCL12 and CXCR4: Chemokine Fuel for Breast Cancer Tumorigenesis. *Cancers* **2020**, *12*, 3071. https://doi.org/10.3390/cancers12103071.
25. Zhao, C.; Wu, M.; Zeng, N.; Xiong, M.; Hu, W.; Lv, W.; Yi, Y.; Zhang, Q.; Wu, Y. Cancer-associated adipocytes: emerging supporters in breast cancer. *J. Exp. Clin. Cancer Res.* **2020**, *39*, 156. https://doi.org/10.1186/s13046-020-01666-z.
26. Wang, Y.; Ren, S.; Wang, Z.; Wang, Z.; Zhu, N.; Cai, D.; Ye, Z.; Ruan, J. Chemokines in bone-metastatic breast cancer: Therapeutic opportunities. *Int. Immunopharmacol.* **2020**, *87*, 106815. https://doi.org/10.1016/j.intimp.2020.106815.
27. Schrörs, B.; Boegel, S.; Albrecht, C.; Bukur, T.; Bukur, V.; Holtsträter, C.; Ritzel, C.; Manninen, K.; Tadmor, A.D.; Vormehr, M.; et al. Multi-Omics Characterization of the 4T1 Murine Mammary Gland Tumor Model. *Front. Oncol.* **2020**, *10*, 1195. https://doi.org/10.3389/fonc.2020.01195.
28. Ingalls, A.M.; Dickie, M.M.; Snell, G.D. Obese, a new mutation in the house mouse. *J. Hered.* **1950**, *41*, 317–318. https://doi.org/10.1093/oxfordjournals.jhered.a106073.
29. Delort, L.; Bougaret, L.; Cholet, J.; Vermerie, M.; Billard, H.; Decombat, C.; Bourgne, C.; Berger, M.; Dumontet, C.; Caldefie-Chezet, F. Hormonal Therapy Resistance and Breast Cancer: Involvement of Adipocytes and Leptin. *Nutrients* **2019**, *11*, 2839. https://doi.org/10.3390/nu11122839.
30. Park, J.Y.; Kang, S.E.; Ahn, K.S.; Um, J.Y.; Yang, W.M.; Yun, M.; Lee, S.G. Inhibition of the PI3K-AKT-mTOR pathway suppresses the adipocyte-mediated proliferation and migration of breast cancer cells. *J. Cancer* **2020**, *11*, 2552–2559. https://doi.org/10.7150/jca.37975.
31. Balaban, S.; Shearer, R.F.; Lee, L.S.; van Geldermalsen, M.; Schreuder, M.; Shtein, H.C.; Cairns, R.; Thomas, K.C.; Fazakerley, D.J.; Grewal, T.; et al. Adipocyte lipolysis links obesity to breast cancer growth: adipocyte-derived fatty acids drive breast cancer cell proliferation and migration. *Cancer Metab.* **2017**, *5*, 1. https://doi.org/10.1186/s40170-016-0163-7.
32. Liu, L.; Wu, Y.; Zhang, C.; Zhou, C.; Li, Y.; Zeng, Y.; Zhang, C.; Li, R.; Luo, D.; Wang, L.; et al. Cancer-associated adipocytes-derived G-CSF promotes breast cancer malignancy via Stat3 signaling. *J. Mol. Cell. Biol.* **2020**, 12, 723–737. https://doi.org/10.1093/jmcb/mjaa016.
33. Song, X.; Zhou, X.; Qin, Y.; Yang, J.; Wang, Y.; Sun, Z.; Yu, K.; Zhang, S.; Liu, S. Emodin inhibits epithelial-mesenchymal transition and metastasis of triple negative breast cancer via antagonism of CC-chemokine ligand 5 secreted from adipocytes. *Int. J. Mol. Med.* **2018**, *42*, 579–588. https://doi.org/10.3892/ijmm.2018.3638.
34. D'Esposito, V.; Liguoro, D.; Ambrosio, M.R.; Collina, F.; Cantile, M.; Spinelli, R.; Raciti, G.A.; Miele, C.; Valentino, R.; Campiglia, P.; et al. Adipose microenvironment promotes triple negative breast cancer cell invasiveness and dissemination by producing CCL5. *Oncotarget* **2016**, *7*, 24495–24509. https://doi.org/10.18632/oncotarget.8336.
35. Blücher, C.; Iberl, S.; Schwagarus, N.; Müller, S.; Liebisch, G.; Höring, M.; Hidrobo, M.S.; Ecker, J.; Spindler, N.; Dietrich, A.; et al. Secreted Factors from Adipose Tissue Reprogram Tumor Lipid Metabolism and Induce Motility by Modulating PPARα/ANGPTL4 and FAK. *Mol. Cancer Res.* **2020**, *18*, 1849–1862. https://doi.org/10.1158/1541-7786.Mcr-19-1223.

36. Bowers, L.W.; Rossi, E.L.; McDonell, S.B.; Doerstling, S.S.; Khatib, S.A.; Lineberger, C.G.; Albright, J.E.; Tang, X.; deGraffenried, L.A.; Hursting, S.D. Leptin Signaling Mediates Obesity-Associated CSC Enrichment and EMT in Preclinical TNBC Models. *Mol. Cancer Res.* **2018**, *16*, 869–879. https://doi.org/10.1158/1541-7786.Mcr-17-0508.
37. Yang, D.; Li, Y.; Xing, L.; Tan, Y.; Sun, J.; Zeng, B.; Xiang, T.; Tan, J.; Ren, G.; Wang, Y. Utilization of adipocyte-derived lipids and enhanced intracellular trafficking of fatty acids contribute to breast cancer progression. *Cell Commun. Signal.* **2018**, *16*, 32. https://doi.org/10.1186/s12964-018-0221-6.
38. Gyamfi, J.; Lee, Y.H.; Eom, M.; Choi, J. Interleukin-6/STAT3 signalling regulates adipocyte induced epithelial-mesenchymal transition in breast cancer cells. *Sci. Rep.* **2018**, *8*, 8859. https://doi.org/10.1038/s41598-018-27184-9.
39. Hsieh, C.C.; Wang, C.H.; Huang, Y.S. Lunasin Attenuates Obesity-Associated Metastasis of 4T1 Breast Cancer Cell through Anti-Inflammatory Property. *Int. J. Mol. Sci.* **2016**, *17*. https://doi.org/10.3390/ijms17122109.
40. Mamidi, T.K.K.; Wu, J.; Tchounwou, P.B.; Miele, L.; Hicks, C. Whole Genome Transcriptome Analysis of the Association between Obesity and Triple-Negative Breast Cancer in Caucasian Women. *Int. J. Environ. Res. Public Health* **2018**, *15*, 2338. https://doi.org/10.3390/ijerph15112338.
41. Łukaszewicz-Zając, M.; Pączek, S.; Mroczko, P.; Kulczyńska-Przybik, A. The Significance of CXCL1 and CXCL8 as Well as Their Specific Receptors in Colorectal Cancer. *Cancer Manag. Res.* **2020**, *12*, 8435–8443. https://doi.org/10.2147/cmar.S267176.
42. Do, H.T.T.; Lee, C.H.; Cho, J. Chemokines and their Receptors: Multifaceted Roles in Cancer Progression and Potential Value as Cancer Prognostic Markers. *Cancers* **2020**, *12*, 287. https://doi.org/10.3390/cancers12020287.
43. Rasha, F.; Ramalingam, L.; Menikdiwela, K.; Hernandez, A.; Moussa, H.; Gollahon, L.; Layeequr Rahman, R.; Moustaid-Moussa, N. Renin angiotensin system inhibition attenuates adipocyte-breast cancer cell interactions. *Exp. Cell Res.* **2020**, *394*, 112114. https://doi.org/10.1016/j.yexcr.2020.112114.
44. Kim, J.H.; Kim, K.Y.; Jeon, J.H.; Lee, S.H.; Hwang, J.E.; Lee, J.H.; Kim, K.K.; Lim, J.S.; Kim, K.I.; Moon, E.Y.; et al. Adipocyte culture medium stimulates production of macrophage inhibitory cytokine 1 in MDA-MB-231 cells. *Cancer Lett.* **2008**, *261*, 253–262. https://doi.org/10.1016/j.canlet.2007.11.020.
45. Chandra, R.K.; Au, B. Spleen hemolytic plaque-forming cell response and generation of cytotoxic cells in genetically obese (C57Bl/6J ob/ob) mice. *Int. Arch. Allergy Appl. Immunol.* **1980**, *62*, 94–98. https://doi.org/10.1159/000232498.
46. Chung, H.; Lee, Y.S.; Mayoral, R.; Oh, D.Y.; Siu, J.T.; Webster, N.J.; Sears, D.D.; Olefsky, J.M.; Ellies, L.G. Omega-3 fatty acids reduce obesity-induced tumor progression independent of GPR120 in a mouse model of postmenopausal breast cancer. *Oncogene* **2015**, *34*, 3504–3513. https://doi.org/10.1038/onc.2014.283.
47. Evangelista, G.C.M.; Salvador, P.A.; Soares, S.M.A.; Barros, L.R.C.; Xavier, F.; Abdo, L.M.; Gualberto, A.C.M.; Macedo, G.C.; Clavijo-Salomon, M.A.; Gameiro, J. 4T1 Mammary Carcinoma Colonization of Metastatic Niches Is Accelerated by Obesity. *Front. Oncol.* **2019**, *9*, 685. https://doi.org/10.3389/fonc.2019.00685.
48. Choe, D.; Lee, E.S.; Beeghly-Fadiel, A.; Wilson, A.J.; Whalen, M.M.; Adunyah, S.E.; Son, D.S. High-Fat Diet-Induced Obese Effects of Adipocyte-Specific CXCR2 Conditional Knockout in the Peritoneal Tumor Microenvironment of Ovarian Cancer. *Cancers* **2021**, *13*, 5033. https://doi.org/10.3390/cancers13195033.